BMC Cancer

RESEARCH

Open Access

Proteomics-driven discovery of LCAT as a novel biomarker for liver metastasis in colorectal cancer

Yuyao Wang[1,4†], Zhengbo Yang[2†], Ziqun Li[1,2†], Linglong Huang[2], Shuangshuang Hou[3], Jiaqi Wang[2], Yang Yu[1,2], Jiajun Yin[1,2*] and Ju Wu[2*]

Abstract

Background This study aimed to identify molecular markers that influence liver metastasis in colorectal cancer (CRC) and assess their clinical relevance.

Methods Proteomic analysis compared differential protein expression between CRC patients with liver metastasis (CRLM) and those without (CRNLM). Bioinformatics and survival analyses identified key proteins and validated them using the TCGA database for expression and clinical significance. Clinical and pathological data, along with tissue samples from our center, were used to create tissue microarrays for immunohistochemistry. Logistic regression assessed odds ratios (OR) for molecular markers linked to liver metastasis post-CRC surgery. Stable LCAT knockdown and overexpression CRC cell lines were constructed, and Transwell assays assessed the impact LCAT on cell migration. Nile red staining of these cells validated the effect LCAT on lipid metabolism in CRC cells.

Results Proteomic analysis identified 383 differentially expressed proteins between the CRLM and CRNLM groups (212 upregulated, 171 downregulated). Enrichment analysis linked these proteins to steroid and alcohol metabolism, inflammation, lipoproteins, and HDL particles, with key pathways in cholesterol and retinol metabolism. Lecithin cholesterol acyltransferase (LCAT), an important enzyme in this process, showed higher expression in CRC tissues, with increased LCAT linked to poorer 5-year OS, DSS, and PFI. LCAT expression also increased with tumor stage. Among 119 patients with CRC, preoperative complications, tumor staging, and LCAT scores differed significantly between patients with and without liver metastasis within 3 years post-surgery. LCAT and postoperative CEA levels were independent risk factors for liver metastasis (LCAT OR, 10.221; $P=0.002$; CEA OR, 1.296; $P=0.014$). Western blotting confirmed significantly higher LCAT expression in CRC tissues with liver metastasis. Transwell assays showed that LCAT overexpression enhanced migratory ability, while knockdown inhibited it. Nile red staining revealed increased lipid droplet accumulation in LCAT-overexpressing CRC cells, which was reduced by LCAT knockdown.

Conclusion LCAT, which is involved in lipid metabolism, is an independent risk factor for liver metastasis following CRC surgery, suggesting its potential as a therapeutic target.

†Yuyao Wang, Zhengbo Yang and Ziqun Li contributed equally to this work and should be considered co-first author.

*Correspondence:
Jiajun Yin
yinjiajun@dlu.edu.cn
Ju Wu
wuju@s.dlu.edu.cn
Full list of author information is available at the end of the article

Keywords Colorectal cancer, Liver metastasis, LCAT, Lipid metabolism

Background

According to the latest global cancer statistics, the incidence and mortality rates of colorectal cancer (CRC) have reached 10.0% and 9.4%, respectively, ranking third in incidence and second in mortality among all malignant tumors [1]. Although surgery and comprehensive treatment have significantly improved the diagnosis and efficacy of CRC treatment, the overall survival (OS) rate remains relatively low in patients with liver metastasis (LM) [2]. LM is the most common type of distant metastasis, with an estimated 15–25% of patients showing signs of LM at the time of initial diagnosis, and approximately 20–25% of patients developing LM after resection of primary CRC [3, 4]. Furthermore, 40–75% of patients experience recurrence after liver resection [5, 6]. Therefore, in clinical practice, identifying molecular markers that affect the occurrence of LM in CRC is valuable for diagnosis and treatment and is of great significance for both short- and long-term prognosis in patients with CRC.

Recent studies have uncovered numerous molecular markers that influence LM in CRC. In 2021, Xu et al. found that the polycomb protein BMI-1 plays a significant role in CRC LM. Their study revealed that BMI-1 is upregulated in CRC with LM and is associated with stage T4 and depth of invasion. Further cellular and animal studies demonstrated that BMI-1 overexpression promotes CRC invasiveness and epithelial-mesenchymal transition (EMT), suggesting it as a potential molecular target for treating CRC LM (CRCLM) [7]. In 2022, Xi Liu et al. identified a mechanism by which MT2A influences LM in CRC. The study showed that overexpression of MT2A enhances the phosphorylation of MST1, LAST2, and YAP1, which inhibits the Hippo signaling pathway and reduces LM in CRC [8]. In a 2024 study, Zhang et al. demonstrated that SLC14A1 interacts with and stabilizes the TβRII protein, preventing its K48-linked ubiquitination and degradation by Smurf1, thus enhancing the TGF-β/Smad signaling pathway and increasing CRC cell invasiveness. Furthermore, TGF-β1 upregulates SLC14A1 mRNA expression, creating a positive feedback loop. Clinical data analysis revealed that SLC14A1 is upregulated in CRC patients with LM, confirming its potential as a predictive marker for LM in CRC [9].

As tumor research has advanced, an increasing number of studies have highlighted the significant role of cellular metabolism in cancer development [10–12]. Lecithin cholesterol acyltransferase (LCAT) is an enzyme responsible for producing most cholesterol esters in plasma and plays a crucial role in the reverse cholesterol transport process. LCAT activity is essential for the formation of mature high-density lipoprotein (HDL) and the remodeling of HDL particles [13–17]. Traditionally, LCAT has been considered "anti-atherosclerotic"; however, recent studies suggest that LCAT may also play a unique role in cancer. Overexpression of LCAT has been linked to certain cancers, including breast and ovarian cancers, where it may alter lipid metabolism in cancer cells and promote tumor growth and invasion [18–21]. Given the special role of LCAT in cancer, it has emerged as a potential therapeutic target. Inhibition of LCAT activity or its expression may suppress tumor growth. However, the mechanisms by which LCAT affects the intracellular and extracellular lipid microenvironment in CRC, thereby contributing to LM, remain unclear and require further investigation.

In this study, we aimed to identify molecular markers influencing LM after CRC surgery. Using proteomic mass spectrometry (MS), we identified differentially expressed proteins between CRC patients who developed LM after surgery and those who did not. Bioinformatics analysis was employed to select hub proteins, and data from the The Cancer Genome Atlas (TCGA) public tumor database were integrated to validate their expression and clinical significance. We collected clinical data and pathological tissue specimens from CRC patients meeting inclusion criteria at our center and established tissue microarray chips to analyze the clinical value of the hub proteins. Finally, a series of experiments were conducted using tissue samples and tumor cells to explore whether LCAT influences CRC cells, elucidating its mechanisms and identifying potential molecular markers affecting LM in CRC. This research provides valuable guidance for clinical practitioners, aiming to improve diagnosis, treatment plans, and ultimately the prognosis of patients with CRC.

Materials and methods

Proteomics mass spectrometry analysis

Essential solutions were prepared for protein extraction using 25 mM dithiothreitol (DTT), 100 mM iodoacetamide, and a phenol extraction reagent (sucrose). The concentration of extracted proteins was determined using the Bradford protein assay. SDS–polyacrylamide gel electrophoresis was then performed, followed by trypsin digestion, peptide desalting, and high-resolution mass spectrometry analysis using liquid chromatography-tandem mass spectrometry (LC–MS/MS). Detailed experimental methods can be found in Supplementary Material 1.

Tissue microarray fabrication, staining, and scanning

Each tissue specimen was cut into blocks measuring 5×15×15 mm and fixed in formalin. Tissue samples

were dehydrated using an ASP300 automated tissue processor. The dehydrated samples were then embedded in paraffin blocks, which were sectioned into 4 μm thick tissue microarrays using an automated microtome. The prepared tissue microarrays were stained using immunohistochemical methods, and the stained arrays were scanned and quantified using a digital pathology slide scanner to obtain H-score values. Detailed methods for tissue microarray fabrication, staining, and quantitative scanning are provided in Supplementary Material 1.

Enrichment analysis

After identifying differentially expressed proteins, Gene Ontology (GO) and Kyoto Encyclopedia of Genes and Genomes (KEGG) enrichment analyses were conducted using R (R packages AnnotationDbi, org.Hs.eg.db, and ClusterProfiler) to describe their functions. The GO/KEGG functional enrichment process involved using the species protein as the background list and the differential protein list as the candidate list. Enrichment significance of functional sets in the differential protein list was calculated using the hypergeometric distribution test to determine the *P*-value.

Public data sources and analysis

RNA-seq data and clinical information from 698 CRC patients were obtained from TCGA. The cohort was divided into high- and low-expression groups based on the median value for survival analysis. Differential expression between tumor and normal tissues was assessed through comparison of non-matched and matched sample groups. Additionally, the cohort was stratified into four groups based on tumor stage, and differential analysis was conducted to test for expression differences across these groups.

Inclusion and exclusion criteria for the clinical cohort

We retrospectively collected data from patients who underwent curative resection for CRC at our department between January 2011 and December 2019. The inclusion criteria were: (1) a confirmed pathological diagnosis of colorectal adenocarcinoma, (2) curative surgical resection, (3) no history of other malignant tumors, (4) at least three years of follow-up, and (5) complete clinical data. The exclusion criteria were: (1) synchronous distant metastasis at initial diagnosis, (2) LM within 3 months after surgery, (3) distant metastasis to other sites after surgery, and (4) loss to follow-up. Ultimately, 119 patients were enrolled and divided into two groups: (1) the LM group (60 patients), defined as those who developed CRC LM (CRLM) within 36 months after resection of the primary tumor, and (2) the non-LM group (59 patients), defined as those who did not develop distant metastasis (CRC non-LM, CRNLM) within 36 months after resection of the primary tumor [22].

Patient information and grouping

Clinical information included age, sex, preoperative tumor complications, T stage, N stage, tumor size, differentiation grade, vascular and neural invasion, postoperative adjuvant chemotherapy, number of lymph node metastases, and postoperative CEA and CA199 levels (measured three months after surgery). All data were obtained from clinical medical records, examination reports, and pathological materials. This study was approved by the Ethics Committee of Zhongshan Hospital, affiliated with Dalian University (Approval Number: KY2023-002–1).

Follow-up

Follow-up assessments were conducted every three months for the first two years, every six months for the next five years, and annually thereafter. The routine follow-up procedures included: (1) routine physical examinations and blood tests every three months for the first two years, every six months for five years, and annually thereafter; (2) chest radiography and abdominal CT scans every six months for the first two years, and annually thereafter; and (3) gastrointestinal endoscopies annually for the first two years. During follow-up, LM was confirmed using contrast-enhanced CT. Patients without metastasis were followed for at least three years after surgery. The follow-up period was defined as the time from the first day after CRC surgery to the appearance of LM or the end of follow-up.

Quantitative real-time PCR

Total RNA was extracted from CRC tissues and adjacent normal tissues using the TRIzol method, which involves tissue processing, Trizol lysis, chloroform separation, isopropanol precipitation, and ethanol washing. LCAT expression was detected using quantitative PCR (qPCR). The primer concentration was 10 μmol/L, and the reaction conditions were as follows: initial denaturation at 55 °C, denaturation at 95 °C, and annealing/extension at 60 °C for 40 cycles. Data analysis was performed using the $2^{-\Delta\Delta Ct}$ relative quantification method. The experiment was repeated three times, and a P-value < 0.05 was considered indicative of significant differences. For detailed experimental methods, see Supplementary Material 1.

Western blotting

Total protein was extracted from cancer and adjacent normal tissues. Tissue samples were minced, washed with phosphate-buffered saline (PBS), homogenized, and centrifuged in RIPA lysis buffer containing PMSF.

The supernatant was collected and stored at −20 °C. For adherent cells, the same procedure was applied: the cells were washed with PBS, lysed in RIPA buffer containing PMSF on ice, and centrifuged to collect the supernatant for storage. The protein concentration was determined using the Bicinchoninic Acid (BCA) assay kit. Standards and samples were prepared, mixed with BCA working solution, and incubated at 37 °C. Protein concentration was calculated by measuring absorbance with a microplate reader. SDS-PAGE gels (resolved and stacked) were prepared, poured onto glass plates, and dried for later use. For the Western blotting experiment, 50 μg of protein samples were denatured at 100 °C, then subjected to SDS-PAGE. Proteins were transferred to a PVDF membrane, blocked, incubated with primary and secondary antibodies, and visualized using an ECL chemiluminescence substrate to detect protein expression levels. For detailed experimental methods, see Supplementary Material 1.

Construction of LCAT stably expressing cells

The lentiviral packaging process involved transfection and culture of 293 T cells. Prior to transfection, the cells were adjusted to an optimal density and switched to serum-free medium. The miRNA expression vectors pHelper1.0 and pHelper2.0 were then mixed with Lipofectamine 2000 to form transfection complexes, which were added to the cell culture medium. After transfection, the cells were cultured for an additional 48 h. The supernatant was collected and subjected to centrifugation, filtration, and ultracentrifugation to concentrate the virus. The virus was aliquoted and stored at −80 °C. Lentivirus titer determination was performed by infecting cells, selecting stably transfected cells with puromycin, and calculating the number of viable cells. Finally, the lentivirus was used to infect cancer cells. After infection, the medium was replaced, and puromycin was added for selection. LCAT expression was detected using qRT-PCR and Western blotting. For detailed experimental methods, see Supplementary Material 1.

Transwell migration assay

The basement membrane was hydrated for 30 min. A cell suspension was then prepared by serum-starving cells for 12–24 h, digesting with trypsin, centrifuging, washing with PBS, and resuspending in serum-free medium containing bovine serum albumin (BSA) to a concentration of 5×10^5 cells/ml. Next, 100 μL of the cell suspension was added to the upper chamber of the Transwell insert, and 600 μL of medium containing 10% FBS was added to the lower chamber. The cells were cultured for 12–48 h. After the culture period, the cells were fixed with methanol for 30 min and stained with crystal violet. Non-migrated cells were removed by wiping, and five random fields were selected under a microscope to count the migrated cells, which were used to assess migratory capacity.

Nile red staining

CRC cells with either overexpressed or downregulated LCAT were cultured at an optimal density. The cells were washed three times with PBS to remove the culture medium, then fixed with 4% paraformaldehyde for 15 min and washed again with PBS. The cells were incubated with diluted Nile Red staining solution at 37 °C for 15–30 min, followed by washing 2–3 times with PBS to remove unbound dye. The red or orange-yellow fluorescence of intracellular lipid droplets was observed and imaged using a fluorescence microscope (excitation wavelength: 543 nm; emission wavelength: 598 nm), and the experimental results were recorded.

Statistical analysis

Continuous variables that fit a normal distribution are expressed as mean ± standard deviation (mean ± SD), while those not fitting a normal distribution are expressed as median with interquartile range (Median, IQR). Categorical variables are expressed as frequencies and percentages. Differences between two groups were compared using the t-test or chi-square test, and differences among multiple groups were compared using analysis of variance (ANOVA). All tests were two-sided. Survival curves were plotted using the Kaplan–Meier method, and differences between survival curves were compared using the log-rank test. Odds ratios (OR) were calculated using logistic regression. Multivariate logistic regression analysis was performed to assess covariates significantly associated with the univariate analysis results. Statistical analyses were conducted using SPSS (version 27.0; IBM Corp., Armonk, NY, USA) and R (version 4.3.1; R Foundation for Statistical Computing, Vienna, Austria). Statistical significance was defined as $P<0.05$.

Results

Differential protein analysis

Proteomic analysis was conducted on pathological tissues from five CRC patients with LM (CRLM) and five without (CRNLM) within three years post-surgery. Using a P-value <0.05 and a fold change of $|\log2FC|\geq1$, cluster analysis heat maps (Fig. 1A) and volcano plots (Fig. 1B) identified 383 differentially expressed proteins: 212 upregulated and 171 downregulated.

Enrichment analysis

GO and KEGG enrichment analyses were performed on the 383 differentially expressed proteins. The GO

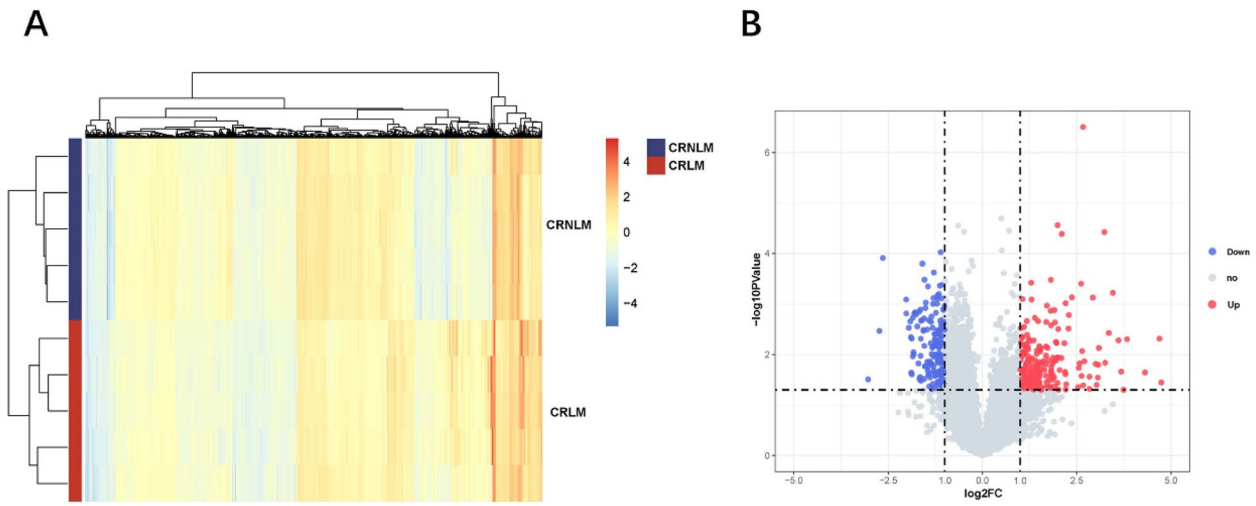

Fig. 1 Differential proteins between the CRLM and CRNLM groups. **A** Cluster Analysis Heatmap: The redder the color, the greater the upregulation of protein expression, and the bluer the color, the greater the downregulation of protein expression. **B** Volcano Plot: Blue dots represent downregulated proteins, red dots represent upregulated proteins, and gray dots represent proteins with no significant difference in expression

enrichment analysis covered three main categories: biological process (BP), cellular component (CC), and molecular function (MF). The results indicated that these proteins were involved in biological processes such as steroid metabolism, alcohol metabolism, and acute inflammatory responses. They were associated with cellular components, including lipoprotein particles, protein-lipid complexes, and HDL particles, and exhibited molecular functions such as lipoprotein particle binding and protein-lipid complex binding (Fig. 2A). KEGG enrichment analysis revealed that these proteins participated in metabolic pathways, including cholesterol metabolism, retinol metabolism, tyrosine metabolism, biosynthesis of steroid hormones, glutathione metabolism, arachidonic acid metabolism, and ferroptosis (Fig. 2B).

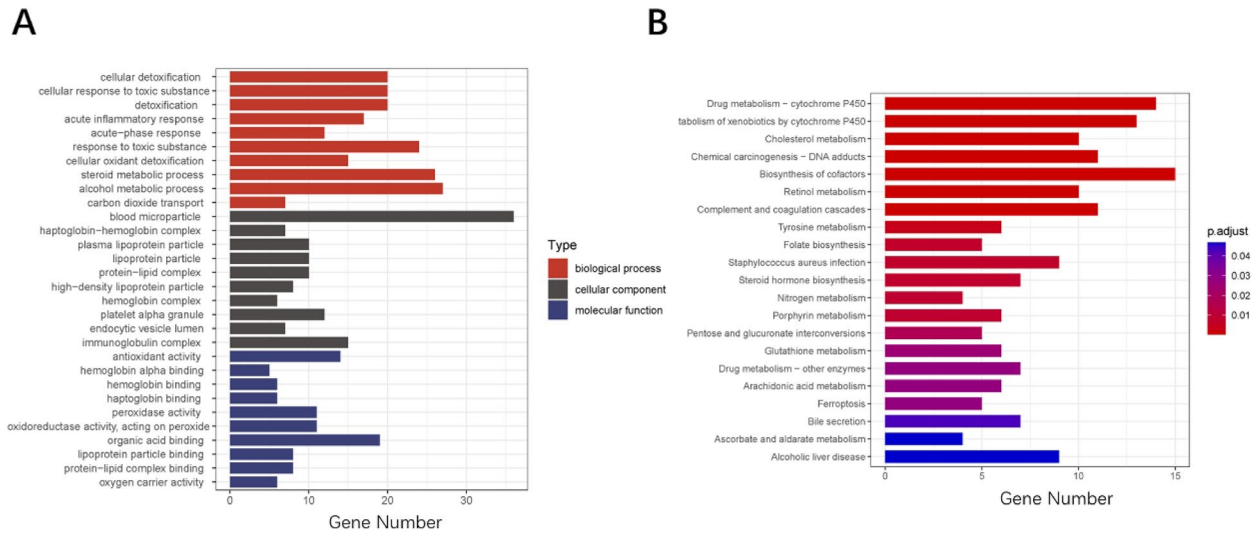

Fig. 2 GO/KEGG enrichment analysis. **A** GO enrichment analysis: red indicates the top five biological processes enriched for differential proteins, gray indicates the top five cellular components enriched for differential proteins, blue indicates the top five molecular functions enriched for differential proteins, and the horizontal axis represents the number of enriched proteins. **B** KEGG enrichment analysis: the redder the color indicates a smaller *P*-value, the bluer the color indicates a larger *P*-value, and the horizontal axis represents the number of enriched proteins

PPI analysis and TCGA database analysis to identify hub proteins

Protein–protein interaction (PPI) network analysis of the differentially expressed proteins was conducted using the STRING website. The Cytoscape software CytoHubba plugin was used to calculate the connectivity of the nodes within the differentially expressed proteins and to identify the top 10 hub proteins (Fig. 3). The hub proteins, ranked from first to tenth, were LCAT, APOA1, SERPINA1, HPX, APOA2, KNG1, C3, AFM, ORM1, and HRG (Supplementary Fig. 1).

The analysis was conducted using transcriptome sequencing data and associated clinical data from 698 patients in the TCGA public database. Survival analysis revealed that LCAT significantly affected the prognosis of patients with CRC. However, APOA1, SERPINA1, HPX, APOA2, KNG1, C3, and ORM1 did not affect CRC prognosis (AFM and HRG had too many missing values in the TCGA database to yield meaningful results) (Supplementary Fig. 2). Differential expression analysis showed that LCAT expression levels in CRC tissues were significantly higher than those in adjacent normal tissues ($P<0.05$) (Supplementary Fig. 3). The 5-year OS (HR = 1.64, 95% CI: 1.16–2.34; Log-rank $P=0.006$), disease-specific survival (DSS) (HR = 1.73, 95% CI: 1.10–2.74; Log-rank $P=0.018$), and progression-free interval (PFI) (HR = 1.49, 95% CI: 1.09–2.03; Log-rank $P=0.012$) were all lower in the high LCAT expression group than in the low LCAT expression group. Analysis of expression differences among tumor pathological stages revealed that LCAT expression levels were significantly higher in more advanced stages ($P<0.05$) (Supplementary Fig. 4).

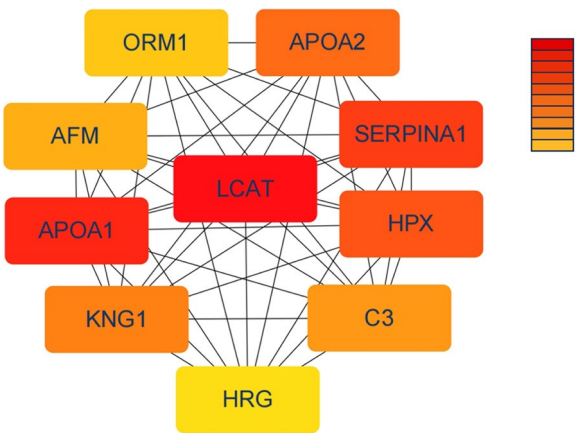

Fig. 3 PPI network interaction analysis. Cytoscape software filters the top 10 hub proteins, with redder colors indicating a higher ranking

The expression level of LCAT was higher in CRLM than in CRNLM

Surgical pathological tissues from 119 patients with CRC were collected for immunohistochemical staining and subsequent scoring. The results of immunohistochemical staining and intergroup scoring are shown in Fig. 4. Patients with CRC who developed LM within three years post-surgery exhibited strong LCAT expression in their tumor tissues, while patients who did not develop LM within three years post-surgery showed weak LCAT expression. A statistically significant difference was observed between the two groups ($P<0.05$). Western blot analysis confirmed that LCAT expression levels in CRLM tumor lesions were significantly higher than those in CRNLM (CRC without LM) (Fig. 5).

Clinical data analysis

We collected clinical data from 60 patients with CRC who developed LM within 3 years after surgery and 59 patients who did not. The clinical baseline data of the patients are presented in Table 1. There were no statistically significant differences in sex, age, postoperative chemotherapy, tumor size, or differentiation degree between the LM and non-LM groups ($P>0.05$). However, significant differences were observed in preoperative tumor complications, T staging, N staging, neurovascular invasion, number of lymph node metastases, postoperative CEA, postoperative CA199, and LCAT scores ($P<0.05$).

The results of the univariate and multivariate logistic regression analyses are presented in Table 2. Preoperative tumor complications, N staging, neurovascular invasion, number of lymph node metastases, postoperative CEA, postoperative CA199, and LCAT scores were identified as statistically significant risk factors for LM after CRC surgery ($P<0.05$). Multivariate logistic regression analysis revealed that LCAT scores (OR: 10.221 [95% CI: 2.287–45.679]; $P=0.002$) and postoperative CEA levels (OR: 1.296 [95% CI: 1.054–1.593]; $P=0.014$) were independent risk factors for LM after CRC surgery ($P<0.05$).

Supplementary Table 1 presents the intergroup differences between the high and low LCAT expression groups. Significant differences were observed between the groups in preoperative tumor complications, T stage, perineural and vascular invasion, LM, and CEA and CA199 levels ($P<0.05$). However, no significant differences were found in age, sex, postoperative chemotherapy, tumor size, degree of differentiation, N stage, or number of lymph node metastases ($P>0.05$).

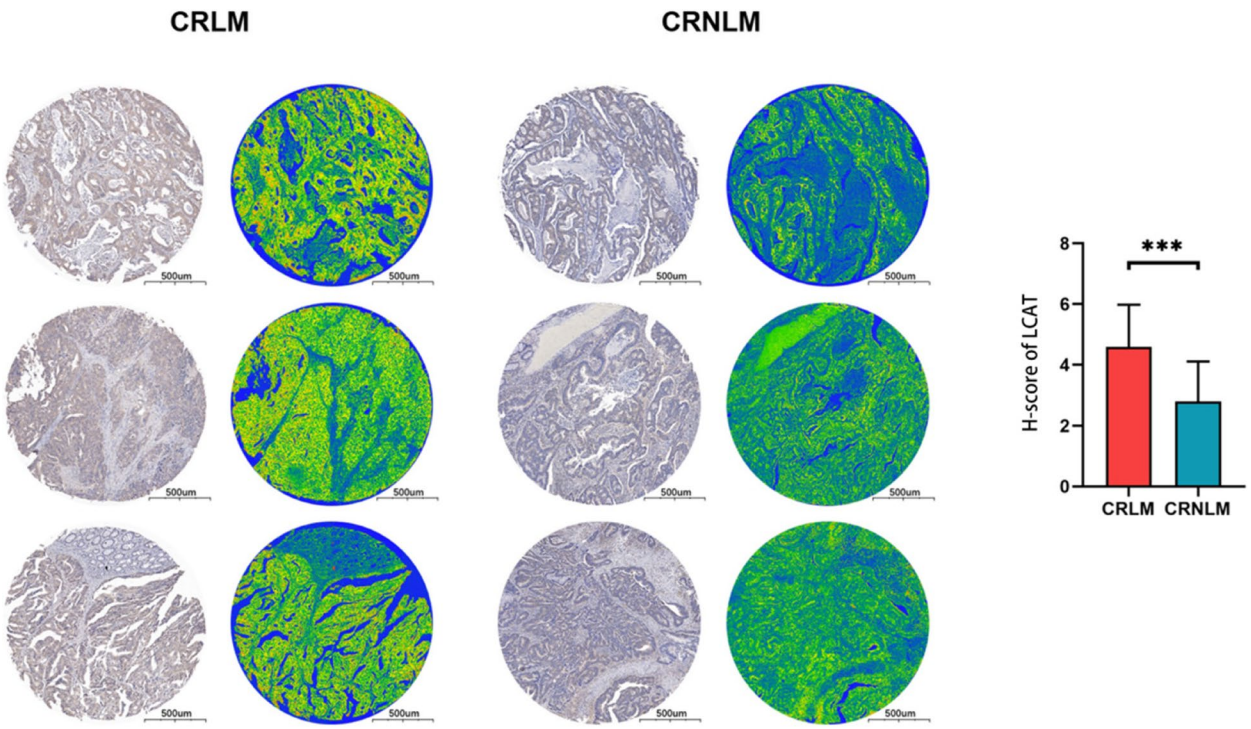

Fig. 4 LCAT staining in the tissue microarray (left). The upper part shows results observed under a microscope, and the lower part shows scanning results. The right side presents the differential H-score analysis of LCAT between the CRLM and CRNLM groups. $P < 0.001$

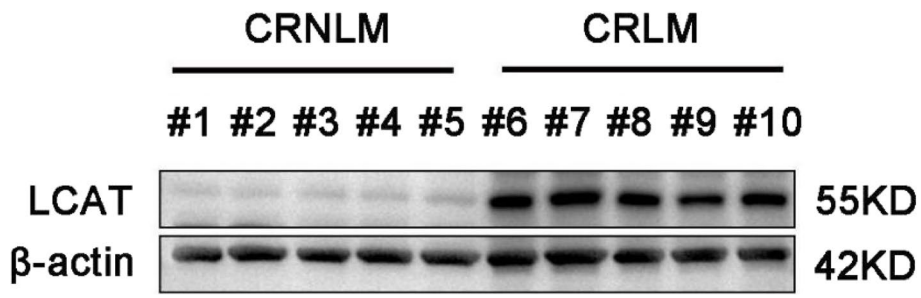

Fig. 5 Western blot analysis showing LCAT protein expression in the CRNLM and CRLM groups. The upper band represents the LCAT protein (approximately 55 kDa), and the lower band represents β-actin (approximately 42 kDa), used as an internal reference. The CRNLM group includes samples #1 to #5, and the CRLM group includes samples #6 to #10

LCAT promotes tumor cell migration by affecting lipid droplet aggregation in CRC

The LOVO cell line was used for LCAT overexpression and knockdown (Supplementary Fig. 5), and Transwell migration assays were performed. The results showed that LOVO cells overexpressing LCAT exhibited significantly enhanced migration, whereas LCAT knockdown in LOVO cells significantly inhibited migration (Fig. 6).

To investigate the mechanisms through which LCAT affects CRC cells, Nile Red staining experiments were conducted. The results showed that CRC cells overexpressing LCAT exhibited more pronounced lipid droplet aggregation, whereas LCAT knockdown significantly reduced lipid droplet aggregation (Fig. 7).

Discussion

Globally, the high incidence and mortality rates of CRC present significant challenges to the medical community. Despite advancements in surgical techniques and integrated therapeutic strategies that have notably improved CRC treatment, enhancing the OS rate of patients with liver metastases remains a complex issue. This study

Table 1 Baseline data table

Characteristics	CRLM	CRNLM	*P* value
n	60	59	
Sex			0.510
Male	32 (53.3%)	35 (59.3%)	
Female	28 (46.7%)	24 (40.7%)	
Age			0.167
< 65	21 (35.0%)	28 (47.5%)	
≥ 65	39 (65.0%)	31 (52.5%)	
Preoperative tumor complications			**< 0.001**
Yes	38 (63.3%)	11 (18.6%)	
No	22 (36.7%)	48 (81.4%)	
Postoperative chemotherapy			0.786
Yes	28 (46.7%)	29 (49.2%)	
No	32 (53.3%)	30 (50.8%)	
Tumor size (cm)			0.119
< 5	22 (36.7%)	30 (50.8%)	
≥ 5	38 (63.3%)	29 (49.2%)	
Degree of differentiation			0.104
Medium–high	52 (86.7%)	57 (96.6%)	
Poorly	8 (13.3%)	2 (3.4%)	
T Stage			**< 0.001**
T3 + T4	59 (98.3%)	43 (72.9%)	
T1 + T2	1 (1.7%)	16 (27.1%)	
N Stage			**< 0.001**
N0	13 (21.7%)	31 (52.5%)	
N +	47 (78.3%)	28 (47.5%)	
Neurovascular infiltration			**< 0.001**
No	31 (51.7%)	48 (81.4%)	
Yes	29 (48.3%)	11 (18.6%)	
Lymph node metastasis	2 (0–5)	0 (0–1)	**< 0.001**
Postoperative CEA(ng/ml)	16.48 (12.47–333.53)	1.53 (0.94–2.47)	**< 0.001**
Postoperative CA199(U/ml)	30.43 (21.13–598.18)	9.31 (6.02–14.87)	**< 0.001**
LCAT	4.69 (3.45–5.81)	3.09 (2.09–3.64)	**< 0.001**

employed proteomic MS to identify differential proteins between patients with CRC who did and did not develop LM after surgery. Through comprehensive bioinformatics analysis, a key hub protein, LCAT, was selected. Our research further utilized data from the public tumor database TCGA to validate the correlation between LCAT expression levels and the clinical characteristics of patients with CRC, providing important molecular evidence for understanding the role of LCAT in CRC LM. Additionally, by collecting and analyzing clinical data and pathological tissues from patients with CRC at our center, we further confirmed the clinical significance of LCAT as a potential molecular marker.

With the continuous advancement of multiomics techniques, significant progress has been made in understanding the molecular mechanisms underlying the LM of CRC. In particular, the role of tumor cell metabolism in CRC LM has gradually emerged. A 2013 study by Thomas et al. revealed significant lipid alterations in tumor regions of CRC LM using imaging MS (IMS) technology, underscoring the key role of lipids in this process [23]. Furthermore, a 2022 study by Wang et al. identified inositol monophosphatase 2 (IMPA2) as a potential hub gene in the occurrence and LM of CRC. Its expression positively correlates with poor prognosis and advanced tumor staging. IMPA2 may influence CRC occurrence and LM by affecting tumor lipid metabolism and the EMT process, as well as regulating its expression through DNA methylation [24]. The findings of this study further expand our understanding of this area. We

Table 2 Logistic univariate and multivariate risk regression

Characteristics	Univariate analysis		Multivariate analysis	
	Odds Ratio (95% CI)	*P* value	Odds Ratio (95% CI)	*P* value
Sex				
Male	Reference			
Female	1.276 (0.617–2.637)	0.510		
Age				
< 65	Reference			
≥ 65	1.677 (0.803–3.504)	0.169		
Preoperative tumor complications				
No	Reference		Reference	
Yes	7.537 (3.255–17.452)	**< 0.001**	4.233 (0.553–32.391)	0.165
Postoperative chemotherapy				
Yes	Reference			
No	0.905 (0.441–1.859)	0.786		
Tumor size(cm)				
< 5	Reference			
≥ 5	1.787 (0.859–3.716)	0.120		
Degree of differentiation				
Medium–high	Reference			
Poorly	4.385 (0.890–21.596)	0.069		
T stage				
T1 + T2	Reference			
T3 + T4	21.953 (2.803–171.929)	0.060		
N stage				
N0	Reference		Reference	
N +	4.003 (1.800–8.899)	**< 0.001**	4.142 (0.471–36.427)	0.200
Neurovascular infiltration				
No	Reference		Reference	
Yes	4.082 (1.784–9.343)	**< 0.001**	0.097 (0.006–1.606)	0.103
Lymph node metastasis	1.214 (1.062–1.387)	**0.004**	1.345 (0.900–2.011)	0.148
Postoperative CEA(ng/ml)	1.263 (1.155–1.381)	**< 0.001**	1.296 (1.054–1.593)	**0.014**
Postoperative CA199(U/ml)	1.068 (1.030–1.106)	**< 0.001**	1.020 (0.966–1.077)	0.475
LCAT	2.804 (1.886–4.167)	**< 0.001**	10.221 (2.287–45.679)	**0.002**

observed significant differences in protein expression patterns between patients who did and did not develop LM after CRC surgery. Pathway enrichment analysis revealed that these differentially expressed proteins were enriched in various metabolic pathways, including cholesterol, retinol, tyrosine, steroid hormone biosynthesis, glutathione, arachidonic acid, and ferroptosis [25–40]. Notably, LCAT, a key enzyme involved in cholesterol esterification and transport, occupied a central position among the significantly altered proteins. In a 2022 study by Zhang et al., LCAT activity in the serum of patients with liver cancer was significantly disrupted compared to that in normal individuals, and LCAT was strongly correlated with prognosis, immune cell infiltration, immune regulatory factors, sensitivity to anticancer drugs, and the proliferation marker KI67 [41]. Moreover, studies by Liang Hong Guoqing Ouyang et al. confirmed the dysregulation of LCAT expression in hepatocellular carcinoma [42, 43].

Through bioinformatics analysis, we found that LCAT expression in CRC samples was significantly higher than in normal tissue samples, and that high LCAT expression was associated with lower OS, disease-free survival, progression-free survival, and advanced tumor staging. This suggests that, after the onset of CRC, changes in LCAT expression may mediate lipid metabolism within or outside tumor cells, thereby influencing tumor biological behavior. A 2020 study by Hyoung-Min Park and colleagues highlighted that LCAT is a biomarker for invasive breast cancer and is highly expressed in late-stage

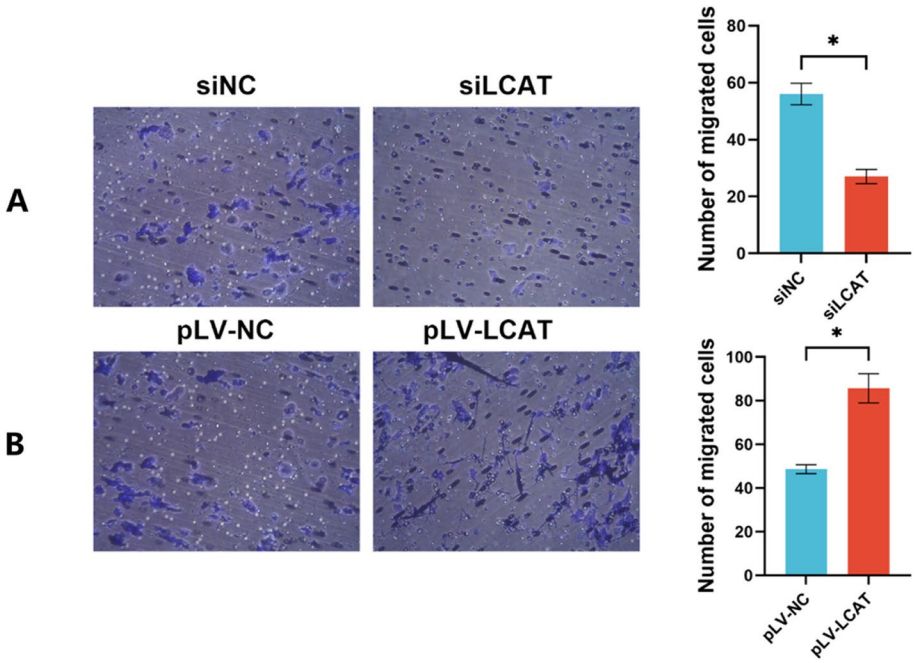

Fig. 6 Panel **A** shows that LCAT knockdown reduced the migratory ability of tumor cells, while Panel **B** shows that LCAT overexpression increased the migratory ability of tumor cells ($P < 0.05$)

or highly metastatic tumors [18], further supporting the potential role of LCAT in tumor invasion and metastasis. In this study, we confirmed that CRC tissues with LM post-surgery exhibited significantly higher LCAT expression levels compared to those without LM post-surgery through immunohistochemical staining, Western blot (WB) experiments, and clinical data analysis. Univariate and multivariate regression analyses identified LCAT as an independent risk factor for LM after CRC surgery. Additionally, through cellular experiments and Nile Red staining, we found that LCAT might promote tumor cell migration by influencing lipid droplet aggregation in CRC cells, thereby affecting lipid metabolism, which ultimately contributes to postoperative LM.

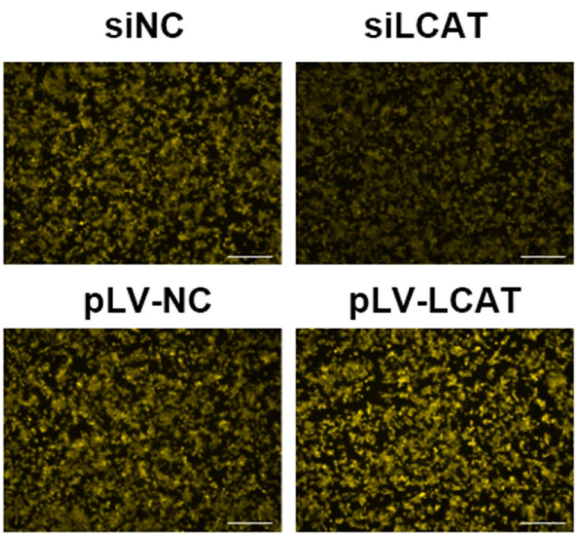

Fig. 7 Nile red staining to validate the impact of siLCAT and pLV-LCAT on lipid droplet aggregation in colorectal cancer cells

Although this study provides new insights into the role of LCAT in LM of CRC, it has several limitations. First, due to the relatively small sample size, there may be a certain degree of selection bias, which could affect the generalizability and applicability of the results. To address this limitation, we plan to expand the sample size in future studies to enhance the statistical power and reliability of our findings. Second, the specific mechanisms underlying the role of LCAT in CRC LM were not verified through animal experiments in this study. Therefore, follow-up studies are needed to design and implement a series of basic experiments to explore how LCAT affects LM in CRC.

Despite these limitations, this study is the first to reveal that LCAT is a potential molecular marker of LM in CRC. By influencing lipid metabolism in CRC cells, LCAT may promotes LM, offering a new perspective for clinical treatment. This not only provides clinicians with a potential therapeutic target but also brings new treatment strategies and hope for patients. We look forward to conducting prospective multicenter studies in the

future to further validate the clinical value of LCAT as a biomarker and to provide higher-level evidence and practical guidance for the clinical diagnosis and treatment of patients with CRC LM.

Conclusion

Our study identified LCAT as a crucial molecular biomarker of LM in CRC. LCAT serves as an independent risk factor for postoperative LM in patients with CRC, potentially by influencing lipid metabolism in CRC cells, thereby facilitating the development of LM after surgery. This study presents a novel therapeutic target for cancer patients and offers a predictive value for the occurrence of postoperative LM.

Abbreviations

ANOVA	Analysis of variance
BP	Biological process
CC	Cellular component
CRC	Colorectal cancer
CRLM	Cancer liver metastasis
CRNLM	CRC patients without liver metastasis
EMT	Epithelial-mesenchymal transition
GO	Gene Ontology
HDL	High-density lipoprotein
IMS	Imaging mass spectrometry
KEGG	Kyoto Encyclopedia of Genes and Genomes
LCAT	Lecithin cholesterol acyltransferase
LM	Liver metastasis
MF	Molecular function
MS	Mass spectrometry
OR	Odds ratios
OS	Overall survival
PBS	Phosphate-buffered saline
PPI	Protein interaction
TCGA	The Cancer Genome Atlas
WB	Western blot

Supplementary Information

The online version contains supplementary material available at https://doi.org/10.1186/s12885-025-13882-x.

Supplementary Material 1.

Supplementary Material 2.

Supplementary Material 3.

Supplementary Material 4.

Acknowledgements

Not applicable.

Authors' contributions

Yuyao Wang and Ju Wu were responsible for the conceptualization of the study. Yuyao Wang and Zhengbo Yang drafted the manuscript and were responsible for the development of the method and software and the visualization of the data. Ziqun Li and Shuangshuang Hou were responsible for the investigation, data collation, review, and editing process. Linglong Huang was responsible for newly added cell experiments. Ziqun Li, Yang Yu and Jiaqi Wang were responsible for validation, formal analysis, and supervision of the project. Jiajun Yin and Ju Wu provided the necessary resources and administered the project. All authors have read and approved the final version of the manuscript.

Funding

This research was funded by the Liaoning Provincial Department of Education Fund (grant number: JYTQN2023104).

Data availability

Public data were available and downloaded from the TCGA website (https://www.cancer.gov/ccg/research/genome-sequencing/tcga). Additional data from this study can be obtained by contacting us via email if necessary.

Declarations

Ethics approval and consent to participate

Ethical approval was granted by the Institutional Ethics Committee of Zhongshan Hospital, which is affiliated with Dalian University (No. KY2023-002–1), and written informed consent was provided before participating in the study. This study was conducted in accordance with the principles of the Declaration of Helsinki.

Consent for publication

Informed consent was obtained from all subjects involved in the study. Written informed consent was obtained from the patients for the publication of this paper.

Competing interests

The authors declare no competing interests.

Author details

[1]Dalian Medical University, Dalian, China. [2]Department of General Surgery, Affiliated Zhongshan Hospital of Dalian University, No. 6 Jiefang Street, Zhongshan District, Dalian 116001, Liaoning Province, China. [3]Department of Surgery, Fuyang Normal University Second Affiliated Hospital, Fuyang, China. [4]Department of Gastrointestinal Surgery, Chengdu Sixth People's Hospital, Chengdu, China.

Received: 15 October 2024 Accepted: 7 March 2025
Published online: 15 March 2025

References

1. Sung H, Ferlay J, Siegel RL, Laversanne M, Soerjomataram I, Jemal A, et al. Global Cancer Statistics 2020: GLOBOCAN Estimates of Incidence and Mortality Worldwide for 36 Cancers in 185 Countries. CA Cancer J Clin. 2021;71:209–49.
2. Tejpar S, Shen L, Wang X, Schilsky RL. Integrating biomarkers in colorectal cancer trials in the West and China. Nat Rev Clin Oncol. 2015;12:553–60.
3. Kopetz S, Chang GJ, Overman MJ, Eng C, Sargent DJ, Larson DW, et al. Improved survival in metastatic colorectal cancer is associated with adoption of hepatic resection and improved chemotherapy. J Clin Oncol. 2009;27:3677–83.
4. Cen B, Lang JD, Du Y, Wei J, Xiong Y, Bradley N, et al. Prostaglandin E2 Induces miR675-5p to Promote Colorectal Tumor Metastasis via Modulation of p53 Expression. Gastroenterology. 2020;158:971-984.e10.
5. Viganò L, Capussotti L, Lapointe R, Barroso E, Hubert C, Giuliante F, et al. Early recurrence after liver resection for colorectal metastases: risk factors, prognosis, and treatment. A LiverMetSurvey-based study of 6,025 patients. Ann Surg Oncol. 2014;21:1276–86.
6. Bhogal RH, Hodson J, Bramhall SR, Isaac J, Marudanayagam R, Mirza DF, et al. Predictors of early recurrence after resection of colorectal liver metastases. World J Surg Oncol. 2015;13:135.
7. Xu Z, Zhou Z, Zhang J, Xuan F, Fan M, Zhou D, et al. Targeting BMI-1-mediated epithelial-mesenchymal transition to inhibit colorectal cancer liver metastasis. Acta Pharm Sin B. 2021;11:1274–85.
8. Liu X, Quan J, Shen Z, Zhang Z, Chen Z, Li L, et al. Metallothionein 2A (MT2A) controls cell proliferation and liver metastasis by controlling the MST1/LATS2/YAP1 signaling pathway in colorectal cancer. Cancer Cell Int. 2022;22:205.

9. Zhang Y, Yang Y, Qi X, Cui P, Kang Y, Liu H, et al. SLC14A1 and TGF-β signaling: a feedback loop driving EMT and colorectal cancer metachronous liver metastasis. J Exp Clin Cancer Res. 2024;43:208.
10. Liu X, Liu Y, Liu Z, Lin C, Meng F, Xu L, et al. CircMYH9 drives colorectal cancer growth by regulating serine metabolism and redox homeostasis in a p53-dependent manner. Mol Cancer. 2021;20:114.
11. Xiong L, Liu H-S, Zhou C, Yang X, Huang L, Jie H-Q, et al. A novel protein encoded by circINSIG1 reprograms cholesterol metabolism by promoting the ubiquitin-dependent degradation of INSIG1 in colorectal cancer. Mol Cancer. 2023;22:72.
12. Sun L, Wan A, Zhou Z, Chen D, Liang H, Liu C, et al. RNA-binding protein RALY reprogrammes mitochondrial metabolism via mediating miRNA processing in colorectal cancer. Gut. 2021;70:1698–712.
13. Albers JJ, Chen CH, Lacko AG. Isolation, characterization, and assay of lecithin-cholesterol acyltransferase. Methods Enzymol. 1986;129:763–83.
14. Fielding CJ, Fielding PE. Molecular physiology of reverse cholesterol transport. J Lipid Res. 1995;36:211–28.
15. Jonas A. Lecithin-cholesterol acyltransferase in the metabolism of high-density lipoproteins. Biochim Biophys Acta. 1991;1084:205–20.
16. Applebaum-Bowden D. Lipases and lecithin: cholesterol acyltransferase in the control of lipoprotein metabolism. Curr Opin Lipidol. 1995;6:130–5.
17. Dobiásová M. Lecithin: cholesterol acyltransferase and the regulation of endogenous cholesterol transport. Adv Lipid Res. 1983;20:107–94.
18. Common plasma protein marker LCAT in aggressive human breast cancer and canine mammary tumor - PubMed. https://pubmed.ncbi.nlm.nih.gov/33298249/. Accessed 18 Jun 2023.
19. Feng Z, Gu Y, Yuan M, Xiao R, Fei Z. Clinical Trials of Liposomes in Children's Anticancer Therapy: A Comprehensive Analysis of Trials Registered on ClinicalTrials.gov. Int J Nanomedicine. 2022;17:1843–50.
20. Russell MR, Graham C, D'Amato A, Gentry-Maharaj A, Ryan A, Kalsi JK, et al. A combined biomarker panel shows improved sensitivity for the early detection of ovarian cancer allowing the identification of the most aggressive type II tumours. Br J Cancer. 2017;117:666–74.
21. Anđelković M, Djordjevic AB, Javorac D, Baralić K, Đukić-Ćosić D, Repić A, et al. Possible role of lead in breast cancer - a case-control study. Environ Sci Pollut Res Int. 2022;29:65211–21.
22. Dou X, Xi J, Zheng G, Ren G, Tian Y, Dan H, et al. A nomogram was developed using clinicopathological features to predict postoperative liver metastasis in patients with colorectal cancer. J Cancer Res Clin Oncol. 2023;149:14045–56.
23. Thomas A, Patterson NH, Marcinkiewicz MM, Lazaris A, Metrakos P, Chaurand P. Histology-driven data mining of lipid signatures from multiple imaging mass spectrometry analyses: application to human colorectal cancer liver metastasis biopsies. Anal Chem. 2013;85:2860–6.
24. Wang L, Liu D, Liu S, Liao T, Jiao Y, Jiang X, et al. Identification of IMPA2 as the hub gene associated with colorectal cancer and liver metastasis by integrated bioinformatics analysis. Transl Oncol. 2022;21: 101435.
25. Holtzman EJ, Yaari S, Goldbourt U. Serum cholesterol and the risk of colorectal cancer. N Engl J Med. 1987;317:114.
26. Jun SY, Brown AJ, Chua NK, Yoon J-Y, Lee J-J, Yang JO, et al. Reduction of Squalene Epoxidase by Cholesterol Accumulation Accelerates Colorectal Cancer Progression and Metastasis. Gastroenterology. 2021;160:1194-1207.e28.
27. Wong CC, Wu J-L, Ji F, Kang W, Bian X, Chen H, et al. The cholesterol uptake regulator PCSK9 promotes and is a therapeutic target in APC/KRAS-mutant colorectal cancer. Nat Commun. 2022;13:3971.
28. Morse MA. The role of glutathione S-transferase P1–1 in colorectal cancer: friend or foe? Gastroenterology. 2001;121:1010–3.
29. Nguyen A, Loo JM, Mital R, Weinberg EM, Man FY, Zeng Z, et al. PKLR promotes colorectal cancer liver colonization through induction of glutathione synthesis. J Clin Invest. 2016;126:681–94.
30. Niu S, Qiu P, Meng J, Tao C, Wen M, Yu N, et al. Light/glutathione-ignited nanobombs integrating azo and tetrasulfide bonds for multimodal therapy of colorectal cancer. J Colloid Interface Sci. 2024;659:474–85.
31. Basu TK, Chan UM, Fields AL, McPherson TA. Retinol and postoperative colorectal cancer patients. Br J Cancer. 1985;51:61–5.
32. Han X, Zhao R, Zhang G, Jiao Y, Wang Y, Wang D, et al. Association of Retinol and Carotenoids Content in Diet and Serum With Risk for Colorectal Cancer: A Meta-Analysis. Front Nutr. 2022;9:918777.
33. Jessup JM, Battle P, Waller H, Edmiston KH, Stolz DB, Watkins SC, et al. Reactive nitrogen and oxygen radicals formed during hepatic ischemia-reperfusion kill weakly metastatic colorectal cancer cells. Cancer Res. 1999;59:1825–9.
34. Nemati M, Hallaj T, Rezaie J, Rasmi Y. Nitrogen and copper-doped saffron-based carbon dots: Synthesis, characterization, and cytotoxic effects on human colorectal cancer cells. Life Sci. 2023;319:121510.
35. Song M, Nishihara R, Cao Y, Chun E, Qian ZR, Mima K, et al. Marine ω-3 Polyunsaturated Fatty Acid Intake and Risk of Colorectal Cancer Characterized by Tumor-Infiltrating T Cells. JAMA Oncol. 2016;2:1197–206.
36. Dai W, Xiang W, Han L, Yuan Z, Wang R, Ma Y, et al. PTPRO represses colorectal cancer tumorigenesis and progression by reprogramming fatty acid metabolism. Cancer Commun (Lond). 2022;42:848–67.
37. Hu A, Wang H, Xu Q, Pan Y, Jiang Z, Li S, et al. A novel CPT1A covalent inhibitor modulates fatty acid oxidation and CPT1A-VDAC1 axis with therapeutic potential for colorectal cancer. Redox Biol. 2023;68:102959.
38. Wolpin BM, Wei EK, Ng K, Meyerhardt JA, Chan JA, Selhub J, et al. Prediagnostic plasma folate and the risk of death in patients with colorectal cancer. J Clin Oncol. 2008;26:3222–8.
39. Kok DE, Steegenga WT, Smid EJ, Zoetendal EG, Ulrich CM, Kampman E. Bacterial folate biosynthesis and colorectal cancer risk: more than just a gut feeling. Crit Rev Food Sci Nutr. 2020;60(2):244–56.
40. Kok DE, van Duijnhoven FJ, Lubberman FJ, McKay JA, van Lanen A-S, Winkels RM, et al. Intake and biomarkers of folate and folic acid as determinants of chemotherapy-induced toxicities in patients with colorectal cancer: a cohort study. Am J Clin Nutr. 2024;119:294–301.
41. Zhang X, Liu X, Zhu K, Zhang X, Li N, Sun T, et al. CD5L-associated gene analyses highlight the dysregulations, prognostic effects, immune associations, and drug-sensitivity predicative potentials of LCAT and CDC20 in hepatocellular carcinoma. Cancer Cell Int. 2022;22:393.
42. Ouyang G, Yi B, Pan G, Chen X. A robust twelve-gene signature for prognosis prediction of hepatocellular carcinoma. Cancer Cell Int. 2020;20:207.
43. Hong L, Zhou Y, Xie X, Wu W, Shi C, Lin H, et al. A stemness-based eleven-gene signature correlates with the clinical outcome of hepatocellular carcinoma. BMC Cancer. 2021;21:716.

Publisher's Note